Journal of
Synchrotron Radiation

ISSN 0909-0495

Received 27 March 2009
Accepted 31 August 2009

A system for measuring elastic wave velocity under high pressure and high temperature using a combination of ultrasonic measurement and the multi-anvil apparatus at SPring-8

Yuji Higo,[a]* Yoshio Kono,[b] Toru Inoue,[b] Tetsuo Irifune[b] and Ken-ichi Funakoshi[a]

[a]Japan Synchrotron Radiation Research Institute, Hyogo 679-5198, Japan, and [b]Geodynamics Research Center, Ehime University, Matsuyama 790-8577, Japan. E-mail: higo@spring8.or.jp

An experimental system to measure the elastic wave velocities of hot-pressed polycrystalline samples at high pressure and high temperature has been installed at SPring-8. It uses a combination of the ultrasonic pulse-echo-overlap method and Kawai-type multi-anvil apparatus (SPEED-1500). X-ray radiographic imaging enables the sample length to be determined at high pressure and high temperature, which is indispensable for precise determination of elastic wave velocity. Precise measurements of the elastic wave velocities of various minerals have been determined at pressures up to 19 GPa and temperatures up to 1673 K. The experimental technique provides the precise elastic wave velocities of various materials corresponding to those in the Earth's mantle.

Keywords: ultrasonic; elastic property; mantle mineral.

1. Introduction

A technique to measure the elastic wave velocity under high pressure and temperature conditions is very important in various fields of science because elastic properties are among the fundamental physical characteristics of materials. In particular, many experimental studies using ultrasonic techniques have been reported in the field of Earth science, because the elasticity of minerals is critical for interpretation of seismic velocity profiles in the Earth's deep interior (*e.g.* Liebermann, 2000). The measurement principle in an ultrasonic method is very simple (the elastic wave velocity is obtained by dividing the length of a sample by the travel time of the ultrasonic wave), and various kinds of samples can be measured (*e.g.* solid, liquid, amorphous). Therefore, ultrasonic measurements in conjunction with high-pressure apparatus have been used for about half a century (Birch, 1960, 1961).

The ultrasonic pulse-echo-overlap method combined with Kawai-type multi-anvil apparatus enables ultrasonic measurements under high pressure exceeding 10 GPa (*e.g.* Yoneda, 1990; Fujisawa & Ito, 1985; Fujisawa, 1998). In these experiments, the ultrasonic transducer was directly attached to the sample or the buffer rod inside the pressure medium. Owing to the large stresses on the transducer, the signal-to-noise ratio of the ultrasonic signal deteriorates rapidly with increasing pressure; in addition, the experimental temperature is limited by about half of the Curie temperature of the piezoelectric transducer (*e.g.* for $LiNbO_3$, T_c = 1406 K) (Turner *et al.*, 1994).

Researchers at SUNY Stony Brook have succeeded in conducting reliable ultrasonic measurements under high pressure by placing the piezoelectric transducer outside the pressure chamber on the outside corner of the anvil (Li *et al.*, 1996; Chen *et al.*, 1996; Flesch *et al.*, 1998). However, the length of the sample under simultaneous high pressure and high temperature may not be accurately determined if it experiences plastic deformation. Under these circumstances, one cannot measure the elastic wave velocity with sufficient accuracy. Recently, researchers at SUNY Stony Brook have successfully developed a technique to precisely determine the length of the sample and the absolute pressure using a combination of the ultrasonic pulse-echo-overlap method and an *in situ* synchrotron X-ray technique in a large-volume multi-anvil apparatus. This has enabled precise measurement of the elastic wave velocity up to 10 GPa and 1600 K (Liebermann & Li, 1998; Chen *et al.*, 1998; Li *et al.*, 1998; Kung *et al.*, 2002, 2004).

Recently, we have transferred the techniques to the high-pressure and high-temperature research beamline (BL04B1) of SPring-8 and developed an ultrasonic measurement system using a multi-anvil apparatus. In this paper we will describe the technical details of the newly developed system, which performed up to 19 GPa and 1673 K.

2. Experimental set-up for ultrasonic measurement

A system for *in situ* ultrasonic measurement at high pressure and high temperature has been installed at BL04B1 in the synchrotron facility of SPring-8. The experimental set-up and

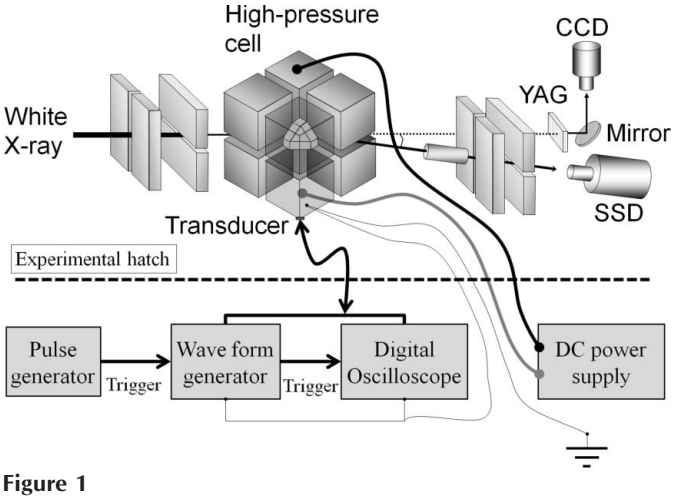

Figure 1
Schematic illustration of the experimental set-up for ultrasonic measurement at BL04B1, SPring-8.

X-ray optics used in the present study are schematically illustrated in Fig. 1. An X-ray radiography system was installed in BL04B1 (Funakoshi *et al.*, 2000) and has been used for a viscosity measurement experiment (Terasaki *et al.*, 2001; Urakawa *et al.*, 2002). A white X-ray beam is directed to the sample, and the transmitted X-rays illuminate a fluorescent YAG crystal. The visible light is then captured with a high-resolution CCD camera *via* an optical mirror. The high-pressure apparatus SPEED-1500 is a uniaxial large-volume press consisting of a Kawai-type high-pressure vessel and two single-axis goniometers (the vertical one is for CCD imaging and the horizontal one is for X-ray diffraction with a 2θ range of 5°) (Utsumi *et al.*, 1998).

The eight second-stage anvils that are compressed by the six first-stage anvils compress an octahedral pressure medium. In the present system, a 26 × 26 × 26 mm tungsten carbide (WC) cube with a truncated edge length of 7 mm was used as the second anvil in this study.

The sample was heated by Joule heating generated by the passage of an electric current through a heater material on the inside of the pressure medium. To prevent deterioration of the signal-to-noise ratio of the ultrasonic signal by the induced current from the usual AC power supply, a DC power supply was used for heating. To prevent fluctuations of the ultrasonic wave signal during heating, the ground of all the devices is taken by one point on the high-pressure apparatus. Electric power control using a personal computer was performed *via* the A/D translation machine, which made it possible to maintain highly precise temperature control (fluctuation in generated temperature is less than 1 K).

A schematic illustration of the cell assemblage used in the combined *in situ* X-ray and ultrasonic measurements is shown in Fig. 2. A hot-pressed polycrystalline specimen was used as a sample. Details of the experimental cell and the procedure are described elsewhere (Higo *et al.*, 2006). The sample was located at the center of a pressure medium and was surrounded by soft NaCl, which prevented distortion of the sample. Gold foils with high X-ray absorption were inserted at

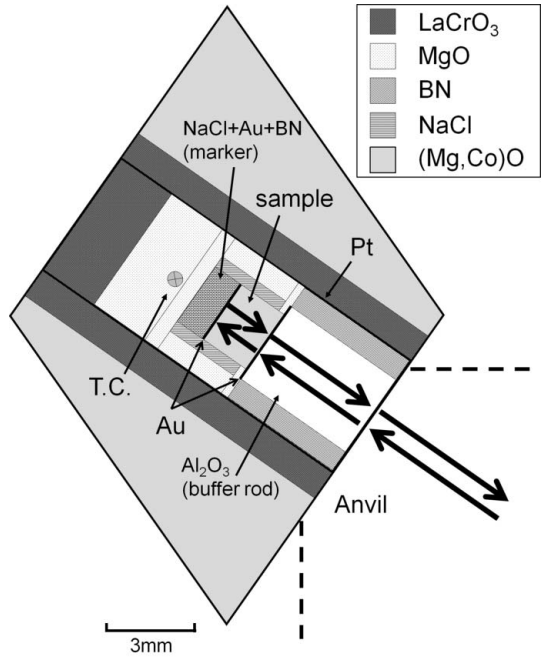

Figure 2
Cross section of the cell assembly used for combined *in situ* X-ray and ultrasonic measurement under high pressure and high temperature. The thick arrows show the direction of the supersonic wave.

both the top and bottom surfaces of the sample. These gold foils improve mechanical coupling between the Al_2O_3 buffer rod and the sample. An ultrasonic wave is transmitted to the sample through the WC anvil and buffer rod. Both ends of the truncated surface of the WC anvil, buffer rod and sample, where the ultrasonic wave propagates, were carefully polished using a 1 μm diamond powder. A cylindrical platinum foil (30 μm thickness) was used as heater material, and the temperature was measured with a $W_{97}Re_3$–$W_{75}Re_{25}$ thermocouple, the hot-junction of which was placed near the backing material. Details of the cell assembly used for ultrasonic experiments are given elsewhere (Higo *et al.*, 2008).

3. Determination of the travel time

The ultrasonic signals were generated and received by the $LiNbO_3$ transducer (10° Y-cut) which can produce both longitudinal and shear waves simultaneously (Kung *et al.*, 2002). A $LiNbO_3$ transducer of thickness 50 μm was pasted on the exposed corner of a WC anvil cube using a bond (EPO-TEK 353ND) (Fig. 3). Since the WC anvil moves during pressurization, the transducer and the electrode were fixed with a conductive epoxy bond, and stable measurement of the ultrasonic wave was enabled under high pressure.

The electrical impedance of the transducer is very low (∼2 Ω) compared with the impedance of a coaxial cable (∼50 Ω). If a coaxial cable is directly connected to an ultrasonic transducer, it becomes a cause by which some signals reflect where the cable and transducer are connected and the signal-to-noise ratio of the ultrasonic signal is worsened. Therefore, a resistor (48 Ω) was connected in series and the

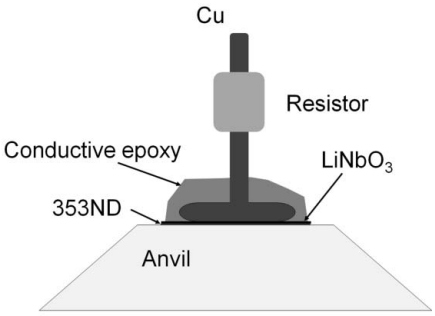

Figure 3
Schematic illustration of the electrode portion of the ultrasonic transducer.

electrical impedance was adjusted to 50 Ω; thus the electrical impedance of the transducer and the coaxial cable were matched, and unnecessary reflection was considerably reduced.

The resonance frequencies of an ultrasonic transducer differ for the longitudinal and shear waves. An electrical sine wave (the frequency is 60 MHz for the longitudinal wave and 40 MHz for the shear wave) with amplitude 5 V_{pp} (V_{pp} = peak-to-peak voltage) was generated by a waveform generator (Tektronix AWG2021). The number of cycles of the sine wave is 3–8. A trigger signal was generated every 2 ms using a pulse generator (Agilent 33250A). The reflected ultrasonic echo was observed with a digital oscilloscope (Tektronix DPO7104). The waveform generator and digital oscilloscope are installed outside of an experiment hatch, which prevents damage by the synchrotron radiation X-rays.

The waveform in real-time acquisition is shown in Fig. 4(*a*). Many electrical noise sources exist in an experiment hatch; the ultrasonic echo signals (V_{pp} < 5 mV) are buried in the noise. Therefore, we adopted double-shielded low-loss-type coaxial cables (RG-217U Fujikura) for the connection between the ultrasonic transducer and the measuring system and equalized about 1000 real-time acquisition data points; consequently, we were able to obtain an ultrasonic echo with a very high signal-to-noise ratio (Fig. 4*b*). The data-collection time of one point was several seconds.

The travel time was measured using the pulse-echo-overlap method. The two-way travel times were measured by shifting the second copy of the echo pattern relative to the original until the bottom end echo and top end echo of the sample overlapped (Fig. 5). In the case of a ringwoodite sample (1.630 mm length), the travel time is about 0.3×10^{-6} s for the longitudinal wave and about 0.5×10^{-6} s for the shear wave (Higo *et al.*, 2008). When the frequency of the ultrasonic wave is 60 MHz, the accuracy of the travel time is not less than one-tenth of the periodic time (1.7×10^{-9} s; ∼0.1% of travel time). The signals were acquired with a sampling rate of 5×10^{9} points s^{-1} (0.2 ns for each data point), which has sufficient resolution for the analysis of an ultrasonic waveform.

The correction in the travel time for the effects of the bond (gold foils) between the sample and the buffer rod was made using the method of Niesler & Jackson (1989). This correction is +1.7 ns for the longitudinal wave and −1.0 ns for the shear wave, corresponding to 0.2–0.5% of the travel time (Higo *et al.*, 2008).

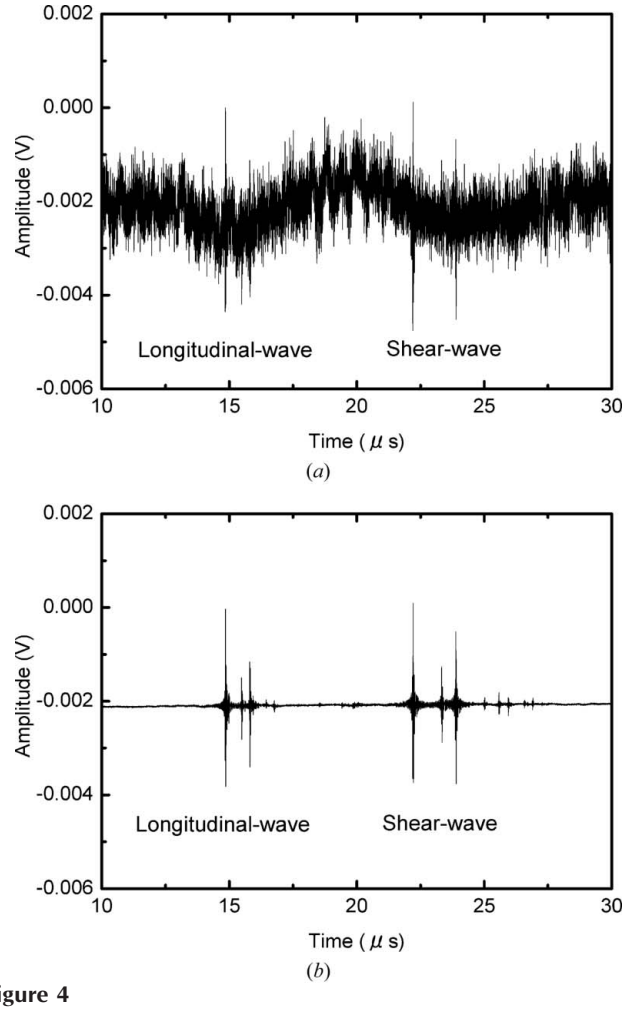

Figure 4
An example of waveform data for P- and S-wave signals under high *P*–*T* conditions (18.0 GPa, 1673 K). (*a*) The waveform acquired in real time. (*b*) Real-time acquisition data equalized ∼1000 times.

4. Determination of sample length

Knowledge of the exact sample length is indispensable for determining the precise elastic wave velocity. The sample length at high pressures was corrected using the internally consistent method developed by Cook (1957) before X-rays were introduced into the ultrasonic experiment (Li *et al.*, 1996). By using *in situ* X-ray diffraction in conjunction with the ultrasonic measurements, it has been possible to infer the sample length (assuming that the bulk sample strain is isotropic and purely elastic) from the measurement of the unit-cell volume at elevated pressures and temperatures (Li *et al.*, 1998; Chen *et al.*, 1998). However, these measurements are not reliable when the sample environments deviate from hydrostatic conditions and plastic deformation occurs at high temperature. Recently, X-ray radiographic imaging techniques have been developed to observe sample lengths directly at high pressures and high temperatures (Kung *et al.*, 2002, 2004).

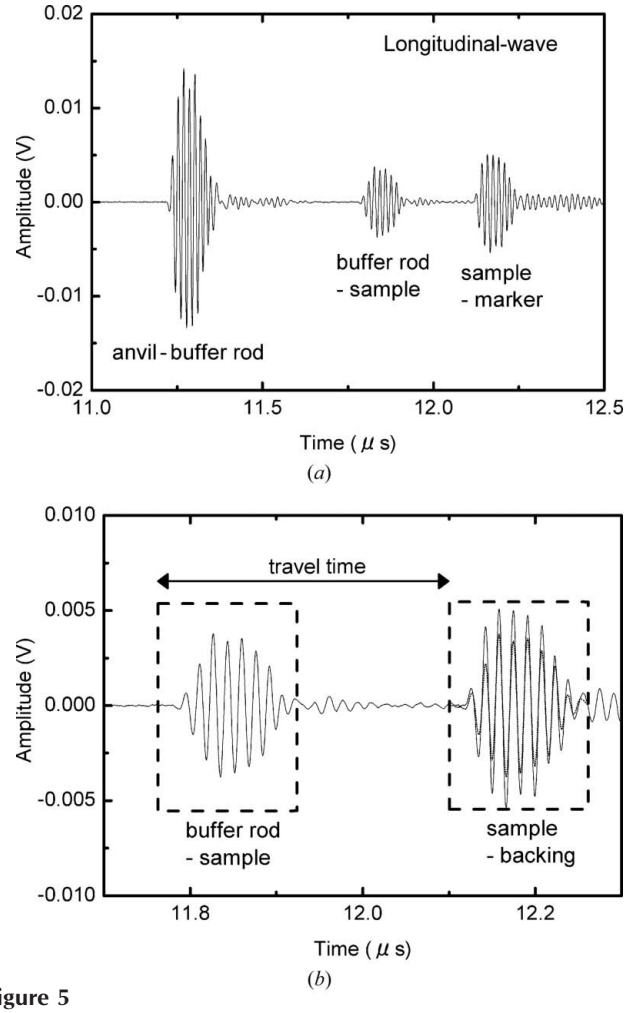

Figure 5
An example of waveform data for longitudinal and shear wave signals at 1673 K and 18.0 GPa. The frequency is 60 MHz. (*a*) Complete view of the ultrasonic echoes of the longitudinal wave. (*b*) Simulation of the pulse-echo-overlap method. The dotted line shows the copying of the echo of the buffer-rod–sample boundary.

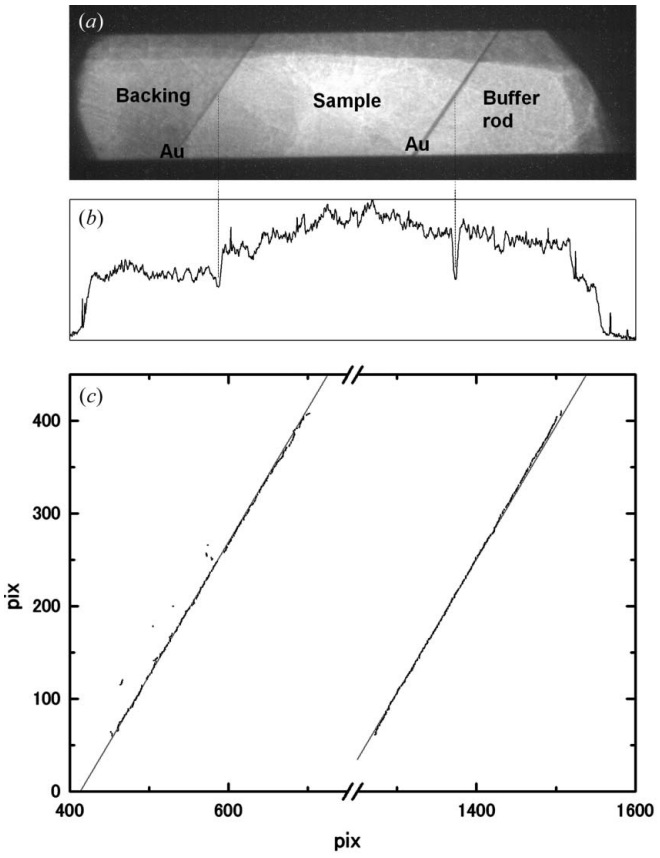

Figure 6
(*a*) An example of the X-ray radiographic image recorded under high *P*–*T* conditions (18 GPa, 1673 K). The upper and lower shadows indicate the WC anvils, whose gap was ∼1 mm under this condition. (*b*) The one-dimensional profile of brightness at the central parts of the radioisotope image of (*a*). (*c*) The position of the dark line detected by image analysis (black dots) and the result of a linear least-squares fitting for the points (gray line). The sample length corresponds to the interval between the two straight lines.

We installed a high-resolution CCD camera (C9300-124, Hamamatsu Photonics) for precise radiography measurement. This high-resolution CCD camera has 4000 (horizontal) × 2672 (vertical) pixels and an effective element area of 36.0 (horizontal) × 23.6 (vertical) mm. This camera was installed immediately after the high-pressure apparatus (about 50 cm downstream from the sample position) to prevent degradation of the image by air scattering of X-rays. The camera's acquisition time is less than 1 s.

The conversion factor between the pixel number of the obtained image and the actual length was estimated at about 2 μm pixel^{-1} using the relationship of the sample position in the X-ray radiography image and displacement of the high-pressure apparatus measured by a linear encoder. Moreover, it is confirmed that the length of the sample under the low-pressure condition calculated by this factor is consistent with the length of the sample before pressurization measured using a precise micrometer.

The X-ray radiographic image is shown in Fig. 6(*a*). As the gold foils preferentially absorb X-rays rather than the alumina buffer rod or the sample, the contrast between the sample and the gold foils is clearly observed on the CCD image. The sample edge is horizontally located in the experiment using a DIA-type high-pressure apparatus (Kung *et al.*, 2002) and a Kawai-type multi-anvil apparatus with a T-cup model (Kung *et al.*, 2004). However, in this system the sample edge leans 54.7° from the horizontal line using the Kawai-type double-stage multi-anvil system with DIA-type high-pressure apparatus. Therefore, the length of the sample was precisely measured by the following procedure.

To position the sample vertical to the incident X-rays, we carefully adjusted the rotation angle of the press stage to zero within a precision of <0.002°. An output file of intensities along the specimen region was obtained for each image (Fig. 6*b*); the specimen region is defined by the discontinuity in intensity at both boundaries, as demarcated by the gold foil. The position of the gold foils identified from the one-dimensional profile of brightness (*e.g.* Fig. 6*b*) is shown in Fig. 6(*c*). The gradient, *a*, and intercept, *b* and *c*, of parallel straight lines can be evaluated by the least-squares method as follows,

$$a = \left[mn\left(\sum_{i=1}^{n}\sum_{j=1}^{n} x_i y_j + \sum_{k=1}^{m}\sum_{l=1}^{m} x_k y_l\right) - \left(m\sum_{i=1}^{n} x_i \sum_{j=1}^{n} y_j + n\sum_{k=1}^{m} x_k \sum_{l=1}^{m} y_l\right)\right] \Big/ \left[mn\left(\sum_{i=1}^{n} x_i^2 + \sum_{k=1}^{m} x_k^2\right) - m\left(\sum_{i=1}^{n} x_i\right)^2 + n\left(\sum_{k=1}^{m} x_k\right)^2\right], \quad (1)$$

$$b = \left\{ \sum_{j=1}^{n} y_j \left[m\sum_{i=1}^{n} x_i^2 + m\sum_{k=1}^{m} x_k^2 - \left(\sum_{k=1}^{m} x_k\right)^2\right] - \sum_{i=1}^{n} x_i \left(m\sum_{i=1}^{n}\sum_{j=1}^{n} x_i y_j + m\sum_{k=1}^{m}\sum_{l=1}^{m} x_k y_l - \sum_{k=1}^{m} x_k \sum_{l=1}^{m} y_l\right)\right\} \Big/ \left[mn\left(\sum_{i=1}^{n} x_i^2 + \sum_{k=1}^{m} x_k^2\right) - m\left(\sum_{i=1}^{n} x_i\right)^2 + n\left(\sum_{k=1}^{m} x_k\right)^2\right], \quad (2)$$

$$c = \left\{ \sum_{l=1}^{m} y_l \left[n\sum_{i=1}^{n} x_i^2 + n\sum_{k=1}^{m} x_k^2 - \left(\sum_{i=1}^{n} x_i\right)^2\right] - \sum_{k=1}^{m} x_k \left(n\sum_{i=1}^{n}\sum_{j=1}^{n} x_i y_j + n\sum_{k=1}^{m}\sum_{l=1}^{m} x_k y_l - \sum_{i=1}^{n} x_i \sum_{j=1}^{n} y_j\right)\right\} \Big/ \left[mn\left(\sum_{i=1}^{n} x_i^2 + \sum_{k=1}^{m} x_k^2\right) - m\left(\sum_{i=1}^{n} x_i\right)^2 + n\left(\sum_{k=1}^{m} x_k\right)^2\right], \quad (3)$$

where (x_i, y_j) and (x_k, y_l) are the positions of the gold foil determined from the one-dimensional profile, and m and n are the number of data. The distance between the two straight lines, which is equivalent to the length of the sample, is given by

$$\text{distance} = \frac{|-b + c|}{(a^2 + 1)^{1/2}}. \quad (4)$$

One pixel corresponds to 2 μm in the present imaging system, and the sample possessed dimensions of 600–800 pixels on X-ray radiographic images. The uncertainties of the above fitting are typically 1–3 pixels; the precision of the sample length is estimated at 0.1–0.3% of the nominal sample length.

An example of sample length change under high-pressure conditions is shown in Fig. 7. The length change estimated from X-ray diffraction data under the assumption of isotropic compression and expansion [in which case $l/l_0 = (V/V_0)^{1/3}$, where l is the sample length and V is the unit-cell volume; zero represents the value at ambient conditions] is also shown in Fig. 7. The sample length determined by X-ray imaging becomes smaller than that estimated from the unit-cell volume with increasing pressure to about 8 GPa, which may be attributed to plastic deformation owing to uniaxial compression of the sample by the hard alumina buffer rod. At pressures higher than 8 GPa, the deviation becomes more significant. Moreover, the length of the sample in the low-pressure condition measured with X-ray radiography and the length of the sample before pressurization have a linear relationship, suggesting that the absolute value of the sample length measured by the X-ray radiography technique is correct. This technique enables us to measure the length of soft material that deforms under high pressure and amorphous material (Kono *et al.*, 2008).

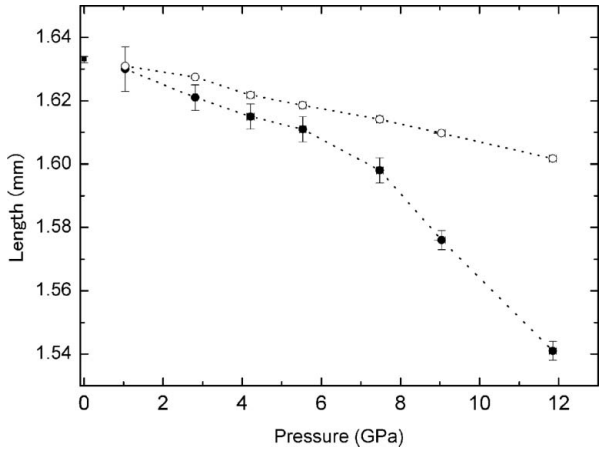

Figure 7
Variations of sample lengths determined by direct measurements from an X-ray radiographic image (filled circles) and estimations from unit-cell volume (open circles) with changing pressure at room temperature. The length of the sample before pressurization was measured using a precise micrometer (filled square).

5. Application to measurement of the elastic wave velocity of minerals in the Earth's mantle

The results of the elastic wave velocity measurement of various materials using this experimental system have recently been published, including measurements of ringwoodite, a high-pressure polymorph of olivine (Higo *et al.*, 2008), majorite, a high-pressure polymorph of pyroxene (Irifune *et al.*, 2008), and mid-ocean-ridge basalt glass (Kono *et al.*, 2008), an analog material of magma in the Earth's mantle. For example, the elastic wave velocities of polycrystalline ringwoodite with an iron content equivalent to that expected in the mantle transition region (Irifune, 1994) have been determined using this technique at pressures up to 19 GPa and temperatures to 1673 K (Higo *et al.*, 2008). The longitudinal and shear wave velocities for the ringwoodite samples are shown in Fig. 8 as a function of pressure and temperature, and are compared with the earlier results by Sinogeikin *et al.* (2003) and Higo *et al.* (2006). The present P- and S-wave velocities are in good agreement with previous studies under high pressure and room temperature; also, the longitudinal and shear wave velocities extrapolated to ambient pressure are in agreement with previous studies under ambient pressure and high temperature. However, the temperature dependence of elastic wave velocity becomes larger at temperatures exceeding 1400 K than in the lower-temperature region (Higo *et al.*, 2008). The present study suggests that the elastic wave velocity should be measured under high-pressure and high-temperature conditions corresponding to the Earth's mantle.

The limits of pressure generated using a Kawai-type multi-anvil apparatus are continually expanding, and pressure

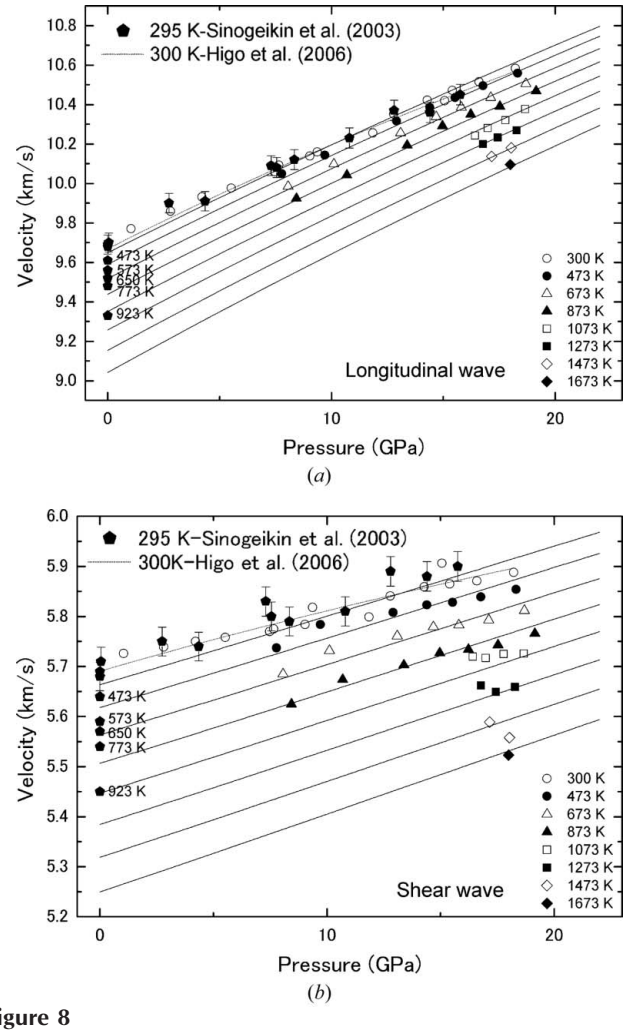

Figure 8
Longitudinal and shear wave velocities of $(Mg_{0.91}Fe_{0.09})_2SiO_4$ ringwoodite at high pressure and high temperature obtained from measurements in the present study. The solid lines show the calculated velocity change from the elastic parameters obtained in this study, where the bulk and shear moduli under high temperature and high pressure are calculated with the multinomial fitting described by Higo *et al.* (2008). The dashed lines are those determined at room temperature by Higo *et al.* (2006), while the small filled pentagons with error bars are the data of Sinogeikin *et al.* (2003).

generation to 80 GPa using a Kawai-type multi-anvil apparatus with a sintered diamond anvil has already been reported (*e.g.* Tange *et al.*, 2008). Combination with the sintered diamond anvil technique may expand the region where ultrasonic experiments are feasible into higher pressures, such as those in the Earth's lower mantle region.

6. Summary

This study reported a system for ultrasonic measurement under high-pressure and high-temperature conditions installed at BL04B1 in SPring-8. With this system, we successfully measured the elastic wave velocity at 19 GPa and up to 1673 K. The pressure and temperature conditions of present elastic wave velocity measurements are higher than those of previous studies using a cubic-type multi-anvil apparatus with an ultrasonic technique (*e.g.* Li *et al.*, 1998; Chen *et al.*, 1998), which was limited to 10 GPa and 1600 K.

Our experimental technique provides us with precise elastic wave velocities of various materials corresponding to those in the Earth's mantle.

The authors thank B. Li, J. Kung, I. Jackson and R. C. Liebermann for invaluable advice and suggestions on installation of the ultrasonic measurement system. The authors thank all members of the Geodynamics Research Center, Ehime University, for help with the *in situ* X-ray experiment at SPring-8 (2004A0465-ND2b-np and 2005A2431-CD2b-np). This work is supported by a Grant-in-Aid for the 'Stagnant Slab Project' from the Japanese government. We thank anonymous reviewers for their thoughtful comments and suggestions that helped to significantly improve the manuscript.

References

Birch, F. (1960). *J. Geophys. Res.* **65**, 1083–1102.
Birch, F. (1961). *J. Geophys. Res.* **66**, 2199–2224.
Chen, G., Li, B. & Liebermann, R. C. (1996). *Science*, **272**, 979–980.
Chen, G., Liebermann, R. C. & Weidner, D. J. (1998). *Science*, **280**, 1913–1916.
Cook, R. K. (1957). *J. Acoust. Soc. Am.* **29**, 445–449.
Flesch, L. M., Li, B. & Liebermann, R. C. (1998). *Am. Mineral.* **83**, 444–450.
Fujisawa, H. (1998). *J. Geophys. Res.* **103**, 9591–9608.
Fujisawa, H. & Ito, E. (1985). *J. Appl. Phys.* **24** (Suppl. 1–24), 103–105.
Funakoshi, K., Kanzaki, M., Yasuda, A., Suzuki, A., Terasaki, H. & Yamashita, S. (2000). *International Conference on High Pressure Science & Technology – AIRAPT-17*, edited by M. H. Manghnani, W. J. Nellis & M. F. Nicol, pp. 1023–1026. Hyderabad: University Press.
Higo, Y., Inoue, T., Irifune, T., Funakoshi, K. & Li, B. (2008). *Phys. Earth Planet. Inter.* **166**, 167–174.
Higo, Y., Inoue, T., Li, B., Irifune, T. & Liebermann, R. C. (2006). *Phys. Earth Planet. Inter.* **159**, 276–285.
Irifune, T. (1994). *Nature (London)*, **370**, 131–133.
Irifune, T., Higo, Y., Inoue, T., Kono, Y., Ohfuji, H. & Funakoshi, K. (2008). *Nature (London)*, **451**, 814–817.
Kono, Y., Ohfuji, H., Higo, Y., Ymada, A., Inoue, T., Irifune, T. & Funakoshi, K. (2008). *J. Mineral. Petrol. Sci.* **103**, 126–130.
Kung, J., Li, B., Uchda, T., Wang, Y., Neuville, D. & Liebermann, R. C. (2004). *Phys. Earth Planet. Inter.* **141**, 27–44.
Kung, J., Li, B., Weidner, D. J., Zhang, J. & Liebermann, R. C. (2002). *Earth Planet. Sci. Lett.* **203**, 557–566.
Li, B., Jackson, I., Gasparik, T. & Liebermann, R. C. (1996). *Phys. Earth Planet. Inter.* **98**, 79–91.
Li, B., Liebermann, R. C. & Weidner, D. J. (1998). *Science*, **281**, 675–677.
Liebermann, R. C. (2000). *Earth's Deep Interior: Mineral Physics and Tomography From the Atomic to the Global Scale, Geophysical Monograph 117*, edited by S. Karato, A. M. Forte, R. C. Liebermann, G. Masters and L. Stixrude, pp. 181–199. Washington, DC: American Geophysical Union.
Liebermann, R. C. & Li, B. (1998). *Ultrahigh-Pressure Mineralogy: Physics and Chemistry of the Earth's Deep Interior*, edited by R. Hemley, Vol. 37, pp. 459–492. Washington, DC: Mineralogical Society of America.
Niesler, H. & Jackson, I. (1989). *J. Acoust. Soc. Am.* **86**, 1573–1585.

Sinogeikin, S. V., Bass, J. D. & Katsura, T. (2003). *Phys. Earth Planet. Inter.* **136**, 41–66.
Tange, Y., Irifune, T. & Funakoshi, K. (2008). *High Press. Res.* **28**, 245–254.
Terasaki, H., Kato, T., Urakawa, S., Funakoshi, K., Suzuki, A., Okada, T., Maeda, M., Sato, J., Kubo, T. & Kasai, S. (2001). *Earth Planet. Sci. Lett.* **190**, 93–101.
Turner, R. C., Fuierer, P. A., Newnham, R. E. & Shrout, T. R. (1994). *Appl. Acoust.* **41**, 299–324.
Urakawa, S., Terasaki, H., Funakoshi, K., Kato, T. & Suzuki, A. (2002). *Am. Mineral.* **86**, 578–582.
Utsumi, W., Urakawa, S., Yamashita, M., Tsiji, K., Konishi, H. & Shimomura, O. (1998). *Rev. High Press. Sci. Technol.* **7**, 1484–1486.
Yoneda, A. (1990). *J. Phys. Earth*, **38**, 19–55.